IEEE Access
Multidisciplinary | Rapid Review | Open Access Journal

Received 29 August 2024, accepted 12 September 2024, date of publication 18 September 2024,
date of current version 30 September 2024.

Digital Object Identifier 10.1109/ACCESS.2024.3463473

RESEARCH ARTICLE

A Post-Processing Histogram Compensation Method for SPAD-Based d-ToF LiDAR Systems for High Photon Flux Measurements

ALESSANDRO TONTINI[1], (Member, IEEE), SONIA MAZZUCCHI[2,3], ROBERTO PASSERONE[4], (Member, IEEE), AND LEONARDO GASPARINI[1], (Member, IEEE)

[1]Fondazione Bruno Kessler, 38123 Trento, Italy
[2]Department of Mathematics, University of Trento, 38123 Trento, Italy
[3]Istituto Nazionale di Fisica Nucleare-Trento Institute for Fundamental Physics and Applications (INFN-TIFPA), 38123 Trento, Italy
[4]Department of Information Engineering and Computer Science, University of Trento, 38123 Trento, Italy

Corresponding author: Roberto Passerone (roberto.passerone@unitn.it)

This work was supported in part by European Union through NextGenerationEU, Progetti di Ricerca di Rilevante Interesse Nazionale (PRIN) 2022, under Grant 2022Z72Y3K.

ABSTRACT In this study, we introduce a histogram post-processing technique for Single Photon Avalanche Diode (SPAD)-based direct Time of Flight (d-ToF) depth measurement systems, designed to address the nonlinearity inherent in SPAD behavior. The technique has been developed to mitigate the distortion of the histogram of timestamps known as pile-up, which results in non-existing fluctuations of the recorded background and reflected laser light. Because of pile-up, accuracy issues arise in the target depth estimation, ultimately limiting the measurement range. The problem is typically addressed implementing sophisticated algorithms to process the histogram of timestamps, with a direct impact on system complexity, frame rate and power consumption. Our method approximates a linear behavior of the SPAD over time by compensating the histogram of timestamps with its own cumulative distribution function (CDF), thereby producing a linearized histogram even in the presence of intense background illumination or strong laser echo, beyond the commonly recognized limit of 5% detection ratio. We first demonstrate the compensation process with simulations, based on a physical model for the computation of the optical power budget and a numerical engine for the generation of the simulated train of timestamps. In particular, we consider a set of realistic parameters for typical SPAD-based d-ToF sensors, allowing us to validate the compensation method over a wide range of values. Then, we validate the method performance using real data obtained from an existing d-ToF sensor. The experimental validation confirms the validity of the method to mitigate accuracy errors due to pile-up with varying target reflectivities, with an improvement of $\approx 73\%$ and $\approx 57\%$ for Lambertian and retroreflective surfaces, respectively. Finally, we analyze the behavior of the method over three different *ToF* extraction algorithms, demonstrating that the measurement range can be extended by more than 50%. Moreover, thanks to the linear shape of the compensated histogram, even a lightweight and computationally inexpensive *ToF* extraction algorithm as a peak detector can be successfully employed with benefits in terms of system complexity, frame rate and power consumption.

INDEX TERMS Single photon avalanche diode (SPAD), light detection and ranging (LiDAR), direct time of flight (d-ToF).

I. INTRODUCTION AND RELATED WORK

Three-dimensional (3D) imaging with SPAD-based receivers is a promising solution to enable spatial awareness for a wide range of applications in industrial [1], automotive [2], consumer [3] and space [4] sectors. One of the main performance-limiting factors, especially for applications where safety of operations and ranging accuracy are of paramount importance, as in industrial environments, is represented by the pile-up distortion. Pile-up distortion occurs

The associate editor coordinating the review of this manuscript and approving it for publication was Sukhdev Roy.

when multiple photons arrive at the SPAD within a short timeframe, causing the detector to register them as a single photon event. This leads to inaccurate photon counting and timing measurements, affecting the reliability of measurement. This non-ideality becomes evident in the presence of strong background light illumination and changes in target reflectivity, resulting in a reduction of the measurement range and a degradation of the measurement accuracy, respectively. In particular, it arises from the combined nonlinear behavior of the SPAD, the time-to-digital converter (TDC) and the limited amount of memory available on-chip, which limits the detection to usually up to a single photon per laser shot [5], [6], [7]. Despite multi-event timestamping approaches [8], [9] have been proposed to mitigate this effect, the non-linear nature of the detection process still represents a limitation.

The objective of this work, therefore, is to address the performance degradation due to pile-up by means of a low-complexity preprocessing of d-ToF histograms to extract target depth with high accuracy, even under challenging illumination conditions. We achieve this by linearizing the SPAD response over time, effectively mitigating pile-up distortion. In the literature, already several approaches have been proposed in this direction. Cominelli et al. [10] propose a theoretical analysis on a method to overcome pile-up distortion in Time-Correlated Single Photon Counting (TCSPC) setups which is based on the match between the SPAD dead-time and the laser excitation period, which has successively been demonstrated with a dedicated hardware implementation by Farina et al [11]. While effective for TCSPC experiments, this approach proves unsuitable for specific d-ToF applications, such as automotive, due to the typical laser repetition periods lasting on the order of microseconds, consequently yielding excessively long SPAD dead-time values. Gupta et al. [12] propose a method to approximate a linear SPAD response by means of a dedicated acquisition process based on a progressive delay of the SPAD activation instant over the acquisition window. With this approach, however, the performance depends upon the granularity of the time gating shifts, resulting in increased acquisition time and system complexity. Another approach, based on a comprehensive Markov chain modeling of the problem, is proposed by Rapp et al. [13], where measurements with a flux of up to 5 photoelectrons per cycle have been achieved without suffering from pile-up distortion. This approach, however, requires either the estimation of the signal and background intensities, or intensive computational power to implement the proposed histogram correction. In more recent work [14], an approach to obtain a truly linearized SPAD response has been presented, demonstrating the capability to obtain linearized histograms of timestamps for high photon flux and strong pile-up operations or even compute the *ToF* in a histogram-less approach with low amount of resources. The approach, however, works at the expense of a dedicated hardware implementation which emulates a linear SPAD response over time.

In our previous work [15], we proposed a method to linearize the SPAD response in post-processing, thus not affecting the architecture and working principle of an already existing SPAD-based d-ToF sensor. The compensation process approximates a linear behavior of the SPAD detector over time, resulting in increased measurement range and improved measurement accuracy, counterbalancing the negative effects of background light and pile-up distortion. The compensation process can be implemented with low amount of hardware/software resources, and the *ToF* from the resulting histogram can be extracted even with a simple peak detection algorithm, thus speeding up the distance extraction process. The approach has been validated with simulations from a Montecarlo model [16] and with measurements from a real d-ToF sensor [6], demonstrating its effectiveness under strong background and pile-up conditions.

In this paper, we extend and complete that work with an analytical formulation of the compensation process which provides insights on the probability distribution function of the compensated histogram and with a comprehensive set of measurements including also retroreflective surfaces, which validate the approach. The results are also supported and benchmarked with the implementation of three different *ToF* extraction algorithms, with varying levels of complexity and performance, to assess the capability of the proposed method to increase the measurement range.

The paper is organized as follows. In Section II, the compensation process is described in detail together with an analytical formulation of the problem. In Section III, results from both simulations and measurements are presented, while the main limits of the proposed approach are discussed in Section IV. Final considerations are given in Section V.

II. METHOD DESCRIPTION

The proposed histogram compensation process has been designed considering one of the most limiting architectures in terms of background light and pile-up distortion, i.e., a synchronous detection approach with the capability to timestamp at most one photon per laser shot. The main parameters required to describe such a detection approach are reported in Table 1. Note that both background and laser flux intensities (λ_B and λ_S, respectively) are expressed in terms of events per second rather than photons per second. In this way, we account for the final flux of detections at the output of the detector, which depends on all optical and technological parameters (photon detection probability (PDP), fill factor (FF), etc.) involved in the process of optical to electrical conversion.

TABLE 1. Main parameters required to describe the detection approach.

Parameter	Unit	Description
λ_B	s^{-1}	Background events rate
λ_S	s^{-1}	Reflected laser events rate
T_W	s	Laser pulse duration
T_{of}	s	Time of flight

A typical histogram of timestamps from this architecture is shown in Figure 1. The *ToF* acquisition can be split in three intervals. From $t = 0$ up to $T \leq ToF$ the SPAD-based sensor is illuminated by only background light, with intensity λ_B. From $t > ToF$ up to $t \leq ToF + T_W$, also the reflected laser light is present, therefore the rate of events in such interval is indicated by $\lambda_B + \lambda_S$. In the last interval, for $t > ToF + T_W$, the sensor is illuminated again by only background light (λ_B). Therefore, the flux of photons reaching the SPAD can be modeled as the sum of two contributions. The first, due to background light, is described as a Poisson process $(N_B(t))_{t\geq 0}$ with intensity λ_B. The second, due to the reflected laser pulse, can be efficiently approximated as a Poisson process $(N_S(t))_{t\in[ToF, ToF+T_W]}$ with intensity λ_S, starting at time $t = ToF$ when the first reflected photon reaches the SPAD and lasting the duration T_W of the laser pulse. Hence, the overall flux can be modeled by an inhomogeneous Poisson process $N(t) = N_B(t) + N_S(t)$ with time-varying intensity function $\lambda : [0, +\infty) \to \mathbb{R}$ given by:

$$\lambda(t) = \begin{cases} \lambda_B & t \in [0, ToF] \\ \lambda_S + \lambda_B & t \in (ToF, ToF + T_W] \\ \lambda_B & t > ToF + T_W \end{cases}$$

In particular, the cumulative distribution function F of the distribution of the random variable T associated to the time of first photon detection is given by:

$$\begin{aligned} F(t) &= \mathbb{P}(T \leq t) \\ &= \begin{cases} 1 - e^{-\lambda_B t} & t \in [0, ToF] \\ 1 - e^{\lambda_S ToF} e^{-(\lambda_S+\lambda_B)t} & t \in (ToF, ToF + T_W] \\ 1 - e^{-\lambda_S T_W} e^{-\lambda_B t} & t > ToF + T_W \end{cases} \end{aligned} \tag{1}$$

while the associated probability density function f can be obtained as:

$$\begin{aligned} f(t) &= F'(t) \\ &= \begin{cases} \lambda_B e^{-\lambda_B t} & t \in [0, ToF] \\ (\lambda_S+\lambda_B) e^{\lambda_S ToF} e^{-(\lambda_S+\lambda_B)t} & t \in (ToF, ToF+T_W] \\ \lambda_B e^{-\lambda_S T_W} e^{-\lambda_B t} & t > ToF+T_W \end{cases} \end{aligned} \tag{2}$$

The main issue with this approach is the uneven weighting of earlier time bins at the expense of later ones, as the underlying statistical process follows an exponential distribution and at most one photon can be recorded per acquisition. In particular, this has two implications. First, the probability of detection is not constant over time, penalizing the maximum achievable measurement range. This can be understood by computing the analytical expression of the probability of detection (P_{det}) of a photon from the reflected laser light, expressed as $P_{det} = e^{-\lambda_B \cdot ToF} \cdot (1 - e^{-\lambda_S \cdot T_W})$. The second implication is the pile-up distortion effect, i.e., the shape of the histogram of timestamps changes with the intensity of the received laser light, resulting in a loss of measurement accuracy as usually a centroid-based algorithm is employed to improve the *ToF* estimation with sub-bin resolution.

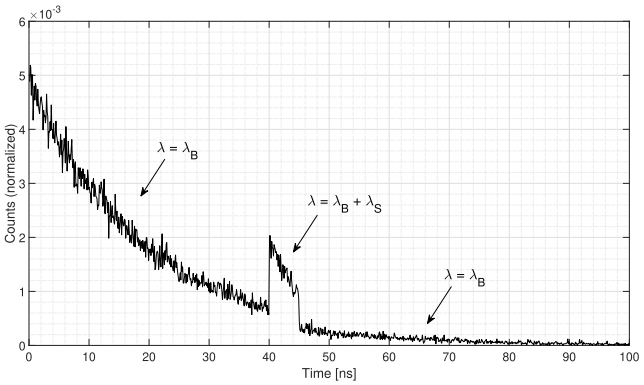

FIGURE 1. Example of histogram of timestamps from a synchronous SPAD-based d-ToF system where the first detected timestamp is recorded. The background light intensity, λ_B, is set to $5 \cdot 10^7$ ph/s, while the reflected laser light intensity, λ_S, is set to 10^8 ph/s. The *ToF* is set to 40 ns and the laser pulse width T_W to 5 ns. The histogram is built using 10^5 timestamps with a bin width of 100 ps. For each region (i.e., before, during and after the laser return), the rate of events (parameter λ of the exponential distribution) is indicated.

For the aforesaid reasons, compensating the histogram of timestamps to restore an equal balancing between earlier and later time bins can improve both measurement range and accuracy. The idea, therefore, is to compensate each bin of the histogram by using its own cumulative distribution function (CDF), by means of a compensation vector C. The value of the compensation vector C for the i-th bin of the original histogram h is computed as follows:

$$C(i) = 1 - \frac{\sum_{k=1}^{i-1} h(k)}{N}, \tag{3}$$

where $\sum_{k=1}^{i-1} h(k)$ is the CDF up to bin $i-1$ and N is the number of measurements composing the histogram h. The compensated histogram h_c is obtained by the element-wise division between the original histogram h and the compensation vector C as follows:

$$h_c = (h \oslash C) \tag{4}$$

This approach can be analytically justified by means of Eq. (1) and (2), noting that the mapping $\tilde{f}$ defined as $\tilde{f}(t) := f(t)/(1 - F(t))$ reduces to the piecewise-constant function

$$\tilde{f}(t) = \begin{cases} \lambda_B & t \in [0, ToF\ ] \cup [ToF + T_W, +\infty) \\ (\lambda_S + \lambda_B) & t \in (ToF, ToF + T_W] \end{cases} \tag{5}$$

In particular, the entries of the compensation vector C defined in Eq. (3) provide the estimate of a discretized version of $(1-F)$. A preliminary validation of the compensation process with a Montecarlo simulation is shown in Figure 2.

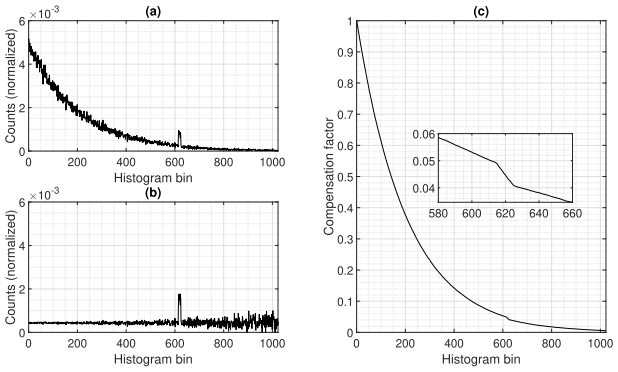

FIGURE 2. Example of histogram compensation in strong pile-up conditions due to background light from Montecarlo simulation. In (a), the original histogram of timestamps is shown, considering a background light intensity, λ_B, of $5 \cdot 10^7$ ph/s, a reflected laser light intensity, λ_S, of $1.5 \cdot 10^8$ ph/s and a pulse duration T_W equal to 1 ns. The *ToF* is set to $\approx$ 60 ns, corresponding to the TDC code $\approx$ 615, with a TDC LSB of $\approx$ 100 ps. The compensated version is shown in (b). The fluctuations appearing after the laser pulse peak (after $t > ToF + T_W$) are due to the lower number of photon counts collected in this region, which ultimately results in wider confidence intervals for the estimates of the theoretical probabilities. In (c), the compensation vector is shown, where a value between 0 and 1 is used for every bin to restore a flat distribution of counts in the final compensated histogram. In the inset, a focus on the region where the laser pulse peak is linearized is shown.

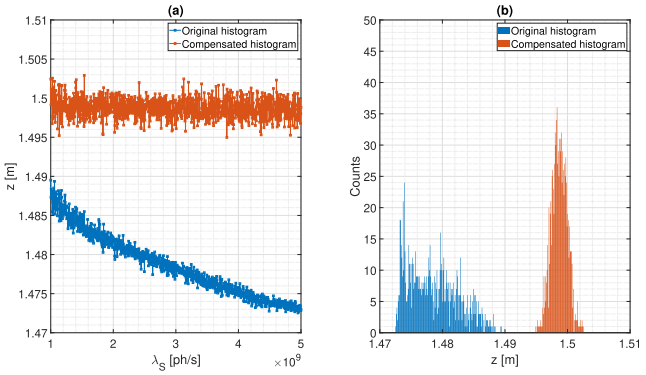

FIGURE 3. Results of Montecarlo simulation to demonstrate the effectiveness in pile-up reduction of the proposed compensation process. We consider a fixed target distance $z = 1.5$ m with a variation of the received laser light intensity λ_S in the range $[1 - 5] \cdot 10^9$ ph/s, typical for single point and scanning approaches facing changes in target reflectivity. In (a) the distance extracted from the original and compensated histograms (blue and red line, respectively) is shown for every value of λ_S. In (b), the distribution of distance measurements is shown, with a reduction in accuracy error from $\approx$ 1.7 cm down to $\approx$ 0.07 cm for the original and compensated histograms, respectively. The background light intensity was set to a challenging $100 \cdot 10^6$ ph/s.

III. CHARACTERIZATION RESULTS

The validation of the proposed histogram compensation process relies on both Montecarlo simulation and measurements. In particular, we consider a d-ToF system with a collimated laser source, thus targeting single-point or scanning approaches, as they represent the typical configuration in industrial environments where measurement accuracy and safety of ranging operations are of paramount importance. Simulations are based on a mixed physical-numerical model as described in our previous work [16]. Measurement have been obtained by using an existing single point d-ToF system, with a SPAD-based sensor similar to the one described in detail in the work by Perenzoni et al. [6]. The performance of the compensation process is evaluated from a set of $2 \cdot 10^3$ *ToF* results. From the dataset, we extract the accuracy error, defined as the difference between the average value of results and the ground truth, and precision, computed as the standard deviation of results.

A. MONTECARLO SIMULATION

With the Montecarlo simulator, we validate the reduction of the accuracy error due to pile-up distortion by configuring a fixed target distance and varying the returning laser echo intensity λ_S. In this way, we simulate a typical scenario where the accuracy is degraded due to pile-up distortion arising from changes in both target topology and reflectivity. In particular, we consider the range $[1 - 5] \cdot 10^9$ events/s for the laser light intensity λ_S while the background light intensity λ_B is set to a challenging $100 \cdot 10^6$ events/s, which, considering the set of optical parameters configured for the simulations, corresponds to $\approx$ 85 kilolux. Figure 3 shows the simulation results, where the accuracy error due to pile-up increases from 1.25 cm to 2.75 cm as the returning laser echo intensity (λ_S) increases. The results demonstrate a reduction of the accuracy error from $\approx$ 1.7 cm down to $\approx$ 0.07 cm for the original and compensated histograms, respectively.

B. ACCURACY ERROR

The objective of the first set of measurements is to verify the capability of the compensation process to reduce the accuracy error due to pile-up distortion in a real measurement setup. In particular, we characterize the compensation process using two different configurations.

In the first configuration we use a white Lambertian target with $\approx$ 90% reflectivity placed at distance of 1.0 m from the sensor. To set different levels of pile-up distortion, the laser light intensity is attenuated by means of several neutral density (ND) filters with optical density (OD) values from 0.0 (no attenuation) up to 0.5 (corresponding to an attenuation of 10). In the second configuration we use a retroreflective target, thus increasing even more the magnitude of pile-up distortion with respect to the white Lambertian target of the previous configuration. Due to the higher reflectivity, measurements have been carried out at a higher distance from the sensor (3.0 m instead of 1.0 m) and using OD values from a minimum of 0.3 up to 1.5. For each configuration we collect and compensate a population of $2 \cdot 10^3$ histograms and we compute the *ToF* with a centroid-based algorithm to extract the resulting accuracy error and precision.

Figure 4 compares the histograms with and without compensation for several values of the attenuation. The results provide a preliminary qualitative assessment, demonstrating that the distortion of the original dataset is recovered in all conditions. A quantitative evaluation, considering the

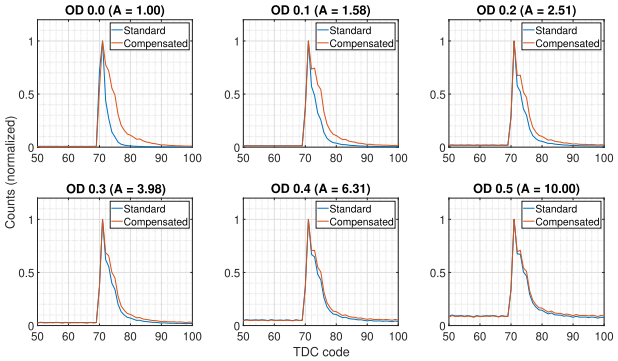

FIGURE 4. Qualitative assessment of the capability of the proposed histogram compensation method to reduce the pile-up error. To attenuate the laser light, we put a set of ND filters with several OD values in front of the laser emitter, to obtain adequate attenuation of the received light. For each plot, we indicate the OD value and the corresponding optical attenuation (A). In contrast to the original histogram (blue line), the width of the compensated histogram (red line) is insensitive to the amount of optical attenuation.

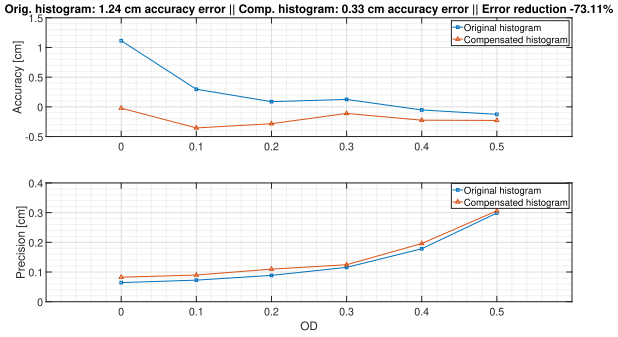

FIGURE 5. Quantitative evaluation of performance improvement of the proposed histogram compensation process in terms of accuracy and precision on a white Lambertian target with ≈ 90% reflectivity. We use a set of OD values in the range 0.0-0.5. The results show that the accuracy improves by ≈ 73% with respect to the original histogram (error from 1.24 cm down to 0.33 cm).

white Lambertian target, is shown in Figure 5. From the obtained results, we demonstrate that the accuracy with the compensated histogram can be improved by ≈ 73%. Results from the retroreflective target are shown in Figure 6, with an improvement in terms of measurement accuracy of ≈ 57%.

C. MEASUREMENT PRECISION

Concerning measurement precision, a careful analysis has to be made to compare results from the compensation process against the standard approach. Within the measurements obtained from the Lambertian target, the amount of pile-up distortion is relatively low, meaning that the echo was not intense enough to saturate the detector completely, and a few counts were observed after the laser pulse. Within the measurements obtained from the Lambertian target, even if the pile-up distortion is relatively low, the *ToF* information is compressed into fewer histogram bins compared to undistorted scenarios, and in particular the compression occurs towards the lowest time bins. This has a

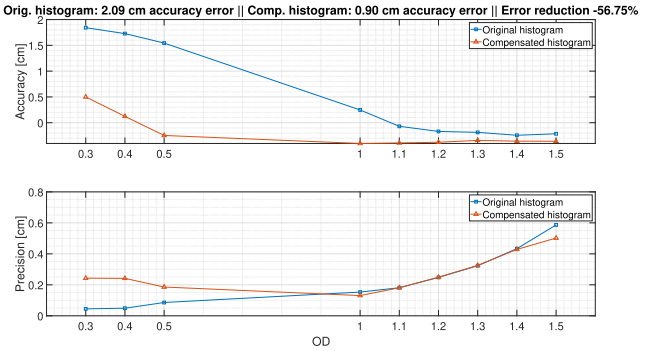

FIGURE 6. Quantitative evaluation of performance improvement of the proposed histogram compensation process in terms of accuracy and precision on a retroreflective surface. We use a set of OD values in the range 0.3-1.5. The results show that and the accuracy improves by ≈ 57% (error from 2.09 cm down to 0.9 cm).

two-fold effect: on the one hand, distance is underestimated, worsening the accuracy, while precision is improved because of the compression effect. This explains the results shown in Figure 5, where the precision achieved with the compensated histogram is slightly lower than that of the original histogram.

In contrast, an extreme case of pile-up distortion is obtained by considering a retroreflective target. In this case, the laser saturates the detector and counts are seldom observed after the laser pulse. For attenuations $\leq$ 0.5, saturation occurs even before the end of the laser pulse, and the compensation fails. The effect of saturation in the compensated histogram is a degradation in the precision for OD <= 0.5, as shown in Figure 6. Then, for higher values of optical attenuation, the two curves tend to be similar, as the echo intensity, despite being strong, does not saturate the detector.

D. MEASUREMENT RANGE

The objective of the second set of measurements is to assess the capability of the histogram compensation process to increase the measurement range. The measurement setup is built using a white Lambertian target moving in steps of 0.5 m on a 1-9 m range. The background light, generated by means of a halogen illuminator coupled to an optical fiber, is pointed directly toward the optical entrance of the sensor, resulting in an equivalent background flux of $\approx 50 \cdot 10^6$ events/s (corresponding to $\approx$ 42.5 kilolux). For each distance we collect $2 \cdot 10^3$ histograms with 10^4 laser shots each, and compute the probability of correct measurement as our evaluation figure of merit. In particular, we consider a distance measurement *correct* if it lies within $\pm 1\%$ of the current distance value. The distance is estimated from both original and compensated histograms using three different *ToF* extraction algorithms, listed below:

- A **centroid-based** algorithm. The *ToF* is computed as the average of the value of N bins centered around the histogram peak, weighted by their respective count. The N bins to be considered in the weighted average computation are set to match the temporal

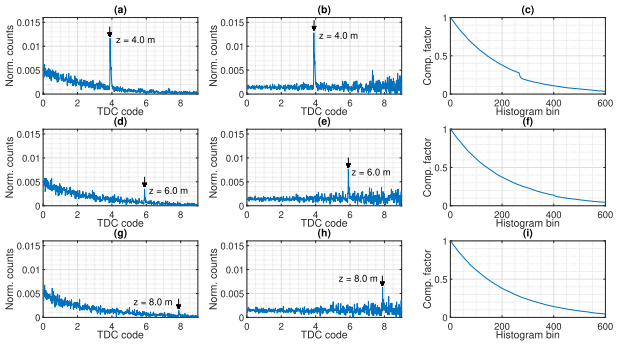

FIGURE 7. Visual comparison between the original and compensated histograms for three distance measurements at 4.0, 6.0 and 8.0 m, respectively. In (a), (b) and (c) the original histogram, the compensated histogram and the compensation vector, respectively, are shown for the measurement at 4.0 m. In (d), (e), (f), and (g), (h), (i), the same is reported for 6.0 m and 8.0 m, respectively. Thanks to the histogram linearization obtained with the compensation process, even a simple and lightweight algorithm as a peak detection to extract the *ToF* information can be successfully used. Conversely, by considering the uncompensated histogram, a peak detection would fail in cases (d) and (g), as the signal peak amplitude is lower than the maximum count from background photons which is located toward the first histogram bins.

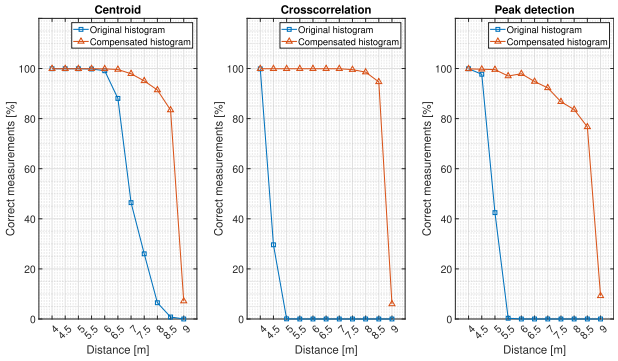

FIGURE 8. Range performance considering three different *ToF* extraction algorithms in the range 1-9 m. Results from 1 m to 4 m are not displayed for the sake of visualization, as the *ToF* from both histograms hits 100% correct measurements. Thanks to the compensated histogram the measurement range can be extended by up to ≈ 4.7 m. Moreover, it is also possible to rely on a simple resource-saving algorithm as the peak detection to extract the target distance.

duration of the laser pulse. In cases of severe pile-up distortion due to background photons, the histogram peak may be located near temporal bins belonging to the background illumination, thus completely jeopardizing the *ToF* extraction. For this reason, before extracting the histogram peak, the derivative of the histogram is computed. In this way, it is more likely to identify the correct peak, corresponding to the edge of counts due to the returning laser pulses.

- A **crosscorrelation-based** algorithm. The *ToF* is extracted by finding the maximum of the crosscorrelation between the histogram and a template of the true laser pulse shape, measured with a calibrated commercial TCSPC setup.
- A **peak detection** algorithm. The *ToF* is extracted by finding the index of the histogram bin with the highest count.

A visual comparison between the original and compensated histograms, for representative distances in the range 4-8.5 m, is shown in Figure 7. A quantitative comparison in terms of probability of correct measurement as a function of the distance is shown in Figure 8. The benefit of the histogram compensation process is twofold. First, ranging performance is improved for each of the *ToF* extraction algorithms selected for the comparison, as opposed to the original histogram approach which clearly shows acceptable results only with the centroid-based approach. Second, the compensated histogram is well suited for an easy and resource-efficient peak detection algorithm, enabling faster and quicker *ToF* acquisitions. By considering a threshold of 80% of the probability of correct measurement, the range can be improved by ≈ 1.9 m with the centroid-based algorithm, by ≈ 4.7 m with the crosscorrelation-based algorithm and by ≈ 3.5 m with the peak detection algorithm.

IV. DISCUSSION

The proposed histogram compensation process allows us to overcome the accuracy degradation due to pile-up distortion and at the same time achieve longer measurement range, leaving more freedom in the choice of several *ToF* extraction algorithms. In this section, we discuss the limits of the proposed approach. First, we focus on the behavior in terms of signal to background ratio (SBR). Somehow counter-intuitively, the SBR does not improve after the compensation process. This aspect can be demonstrated analytically, by extracting the explicit expression of the SBR from the probability density functions (Eq. 2 and 5), as well as with measurements. We define the SBR as the ratio between the average probability of histogram bins in two different regions: one centered around the peak of width equal to the laser pulse duration, and one adjacent to and around the first of width 2δ. More specifically:

$$SBR := \frac{\frac{1}{T_W}\int_{ToF}^{ToF+T_W} f(t)dt}{\frac{1}{2\delta}\left(\int_{ToF-\delta}^{ToF} f(t)dt + \int_{ToF+T_W}^{ToF+T_W+\delta} f(t)dt\right)}. \quad (6)$$

In the case of the compensated histogram, by Eq. (5) one easily gets $SBR = 1 + \frac{\lambda_S}{\lambda_B}$, while for the original histogram Eq. (2) yields

$$SBR = \frac{\frac{1}{T_W} e^{\lambda_B ToF}(1-e^{-(\lambda_S+\lambda_B)T_W})}{\frac{1}{2\delta}\left(e^{-\lambda_b ToF}(e^{-\lambda_B\delta}-1) - e^{-\lambda_S T_W} e^{-\lambda_B(ToF+T_W)(1-e^{-\lambda_B\delta})}\right)} \quad (7)$$

By taking the first order Taylor expansion in powers of T_W and δ, the formula above reduces to $SBR \sim 1 + \frac{\lambda_S}{\lambda_B}$, showing that the two techniques do not present significant differences regarding this parameter. The value of δ can be selected empirically to match the laser pulse width, to account for the background contribution where it has the greatest impact on the SBR. Conversely, after the histogram

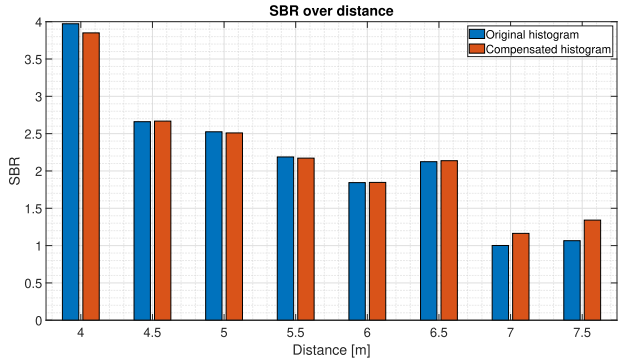

FIGURE 9. SBR computed in the range 4-7 m from the original and compensated histograms, respectively. In accordance to the theoretical analysis, no significant differences can be observed between the two datasets.

compensation, the SBR does not depend on δ anymore, as the count distribution is uniform. The SBR obtained from measured data is reported in Figure 9, showing no significant difference between the original and compensated histograms, as predicted by the theoretical analysis. We quantitatively evaluate this difference by calculating the cosine similarity between the two datasets, yielding a similarity value of 99.87%.

The second limitation of the proposed approach is the potentially high noise in the compensated histogram which arises from the low statistics used to compute the CDF (and thus, the compensation vector C). When the number of counts in the original histogram is particularly low, the estimation of the CDF is affected by statistical uncertainty, resulting in statistical noise amplification in the compensated histogram, which may lead to erroneous depth estimations in presence of low SBR. This can be observed from both simulated data (Figure 2-(b)) and measurements (by observing the compensated histogram tail in Figure 7-(b)). As our method is designed to operate in post-processing, the capability to linearize the SPAD response is intrinsically limited by the amount of photon statistics available with the original histogram of timestamps. A possible countermeasure to mitigate for this limitation is to stop the compensation process after a certain percentage of histogram counts is reached, to avoid compensating histogram regions with insufficient counts to safely estimate the CDF.

V. CONCLUSION

In this work, we demonstrate a lightweight histogram post-processing method to overcome the main limitation of SPAD-based d-ToF systems. The compensation process, which is based on the computation of the CDF of the original histogram, results in a well approximated linearized response over the incoming flux of photons, overcoming the performance degradation due to the pile-up effect and improving the measurement accuracy by $\approx 73\%$ and $\approx 57\%$ for Lambertian and retroreflective target surfaces, respectively. Moreover, the compensated histogram enables successful measurements under challenging background light conditions for a number of different *ToF* extraction algorithms, and thanks to its linear shape, even a lightweight and resource-saving algorithm as a peak detector can be successfully employed.

REFERENCES

[1] V. Sesta, K. Pasquinelli, R. Federico, F. Zappa, and F. Villa, "Range-finding SPAD array with smart laser-spot tracking and TDC sharing for background suppression," *IEEE Open J. Solid-State Circuits Soc.*, vol. 2, pp. 26–37, 2022.

[2] A.-T. Hsiao, C.-H. Liu, P.-H. Chen, Y.-L. Liu, W.-C. Wang, T.-H. Sang, C.-M. Tsai, G. Lin, J.-I. Guo, and S.-D. Lin, "Real-time LiDAR module with 64 × 128-pixel CMOS SPAD array and 940-nm PCSEL," in *Proc. IEEE Sensors Appl. Symp. (SAS)*, Aug. 2022, pp. 1–6.

[3] C. Zhang, N. Zhang, Z. Ma, L. Wang, Y. Qin, J. Jia, and K. Zang, "A 240 × 160 3D-stacked SPAD dToF image sensor with rolling shutter and in-pixel histogram for mobile devices," *IEEE Open J. Solid-State Circuits Soc.*, vol. 2, pp. 3–11, 2022.

[4] F. Villa, F. Severini, F. Madonini, and F. Zappa, "SPADs and SiPMs arrays for long-range high-speed light detection and ranging (LiDAR)," *Sensors*, vol. 21, no. 11, p. 3839, Jun. 2021.

[5] M. Perenzoni, D. Perenzoni, and D. Stoppa, "A 64 × 64-pixels digital silicon photomultiplier direct TOF sensor with 100-MPhotons/s/pixel background rejection and imaging/altimeter mode with 0.14% precision up to 6 km for spacecraft navigation and landing," *IEEE J. Solid-State Circuits*, vol. 52, no. 1, pp. 151–160, Jan. 2017.

[6] M. Perenzoni, N. Massari, L. Gasparini, M. M. Garcia, D. Perenzoni, and D. Stoppa, "A fast 50 × 40-pixels single-point DTOF SPAD sensor with photon counting and programmable ROI TDCs, with σ <4 mm at 3 m up to 18 klux of background light," *IEEE Solid-State Circuits Lett.*, vol. 3, pp. 86–89, 2020.

[7] E. Manuzzato, A. Tontini, A. Seljak, and M. Perenzoni, "A 64 × 64-pixel flash LiDAR SPAD imager with distributed pixel-to-pixel correlation for background rejection, tunable automatic pixel sensitivity and first-last event detection strategies for space applications," in *IEEE Int. Solid-State Circuits Conf. (ISSCC) Dig. Tech. Papers*, vol. 65, Feb. 2022, pp. 96–98.

[8] N. A. W. Dutton, S. Gnecchi, L. Parmesan, A. J. Holmes, B. Rae, L. A. Grant, and R. K. Henderson, "A time-correlated single-photon-counting sensor with 14GS/S histogramming time-to-digital converter," in *IEEE Int. Solid-State Circuits Conf. (ISSCC) Dig. Tech. Papers*, Feb. 2015, pp. 1–3.

[9] S. W. Hutchings, N. Johnston, I. Gyongy, T. Al Abbas, N. A. W. Dutton, M. Tyler, S. Chan, J. Leach, and R. K. Henderson, "A reconfigurable 3-D-Stacked SPAD imager with in-pixel histogramming for flash LiDAR or high-speed time-of-flight imaging," *IEEE J. Solid-State Circuits*, vol. 54, no. 11, pp. 2947–2956, Nov. 2019.

[10] A. Cominelli, G. Acconcia, P. Peronio, M. Ghioni, and I. Rech, "High-speed and low-distortion solution for time-correlated single photon counting measurements: A theoretical analysis," *Rev. Sci. Instrum.*, vol. 88, no. 12, Dec. 2017, Art. no. 123701.

[11] S. Farina, G. Acconcia, I. Labanca, M. Ghioni, and I. Rech, "Toward ultra-fast time-correlated single-photon counting: A compact module to surpass the pile-up limit," *Rev. Sci. Instrum.*, vol. 92, no. 6, Jun. 2021, Art. no. 063702.

[12] A. Gupta, A. Ingle, and M. Gupta, "Asynchronous single-photon 3D imaging," in *Proc. IEEE/CVF Int. Conf. Comput. Vis. (ICCV)*, Oct. 2019, pp. 7908–7917.

[13] J. Rapp, Y. Ma, R. M. A. Dawson, and V. K. Goyal, "High-flux single-photon LiDAR," *Optica*, vol. 8, no. 1, pp. 30–39, Jan. 2021.

[14] A. Tontini, S. Mazzucchi, R. Passerone, N. Broseghini, and L. Gasparini, "Histogram-less LiDAR through SPAD response linearization," *IEEE Sensors J.*, vol. 24, no. 4, pp. 4656–4669, Feb. 2024.

[15] A. Tontini, S. Mazzucchi, N. Brosegini, R. Passerone, and L. Gasparini, "A histogram compensation process for SPAD-based d-ToF LiDAR systems for high photon flux measurements," *Proc. SPIE*, vol. 12998, pp. 246–250, Apr. 2024.

[16] A. Tontini, L. Gasparini, and M. Perenzoni, "Numerical model of SPAD-based direct time-of-flight flash LiDAR CMOS image sensors," *Sensors*, vol. 20, no. 18, p. 5203, Sep. 2020.

ALESSANDRO TONTINI (Member, IEEE) received the M.S. degree in telecommunications engineering and the Ph.D. degree in information and communication technologies from the University of Trento, Italy, in 2017 and 2024, respectively, with a focus on advanced techniques for SPAD-based CMOS d-ToF systems. Since 2017, he has been a Researcher with the Center for Sensors and Devices, Fondazione Bruno Kessler, Trento, focusing on the modeling and development of SPAD-based CMOS image sensors for Time-of-Flight/LiDAR, quantum random number generations, and bio-/medicine applications.

SONIA MAZZUCCHI received the M.S. degree in physics and the Ph.D. degree in mathematics from the University of Trento, Trento, Italy, in 1999 and 2003, respectively. She was an Alexander von Humboldt Fellow at the Institute of Applied Mathematics, University of Bonn, Bonn, Germany. She is currently an Associate Professor in probability and mathematical statistics with the Department of Mathematics, University of Trento. She has published numerous research articles and monographs in the area of stochastic analysis and its applications to quantum mechanics, quantum information, and quantum technologies.

ROBERTO PASSERONE (Member, IEEE) received the M.S. degree in electrical engineering and computer sciences from the Politecnico di Turino, Turin, Italy, in 1994, and the Ph.D. degree in electrical engineering and computer sciences from the University of California at Berkeley, Berkeley, CA, USA, in 2004. He was a Research Scientist at Cadence Design Systems, San Jose, CA, USA. He is currently a Professor in electronics with the Department of Information Engineering and Computer Science, University of Trento, Trento, Italy. He has published numerous research papers in international conferences and journals in the area of design methods for systems and integrated circuits, formal models, and design methodologies for embedded systems. He has served as the general, program, and track chair for various editions of SIES and ETFA and was the Track Chair for DATE. He has participated in several European, national, and industrial projects, and was a Local Coordinator for the University of Trento for ArtistDesign, COMBEST, and CyPhERS.

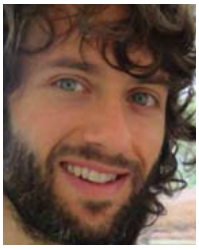

LEONARDO GASPARINI (Member, IEEE) received the Ph.D. degree in information and communication technologies from the University of Trento, Trento, Italy, in 2011, with a focus on ultra-low-power camera systems. Since 2010, he has been a Researcher with the Center for Sensors and Devices, Fondazione Bruno Kessler, Trento, where he is currently the Head of the Integrated Readout-ASICs and Image Sensors (IRIS) Research Unit. Here, he is engaged in the development of CMOS image sensors, including single-photon detector arrays for time-of-flight/LiDAR systems, bio-medicine, particle physics, and quantum optics.

Open Access funding provided by 'Università degli Studi di Trento' within the CRUI CARE Agreement